Journal of Materials Chemistry A

Accepted Manuscript

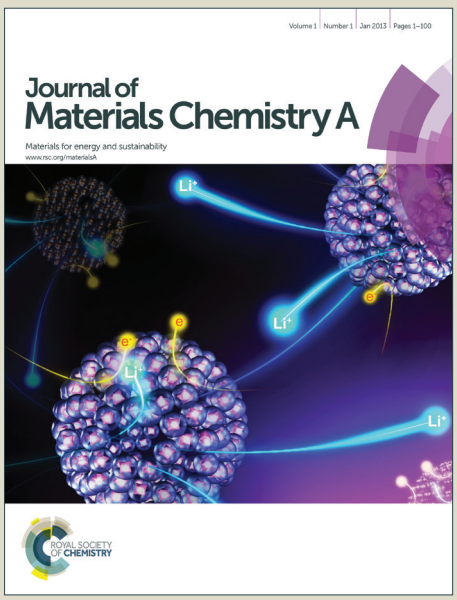

ROYAL SOCIETY OF CHEMISTRY

www.rsc.org/materialsA

Journal Name

RSCPublishing

COMMUNICATION

Supercapacitors based on camphor-derived meso/macroporous carbon sponge electrodes with ultrafast frequency response for ac line-filtering†

Cite this: DOI: 10.1039/x0xx00000x

Received 00th January 2015,
Accepted 00th January 2015

DOI: 10.1039/x0xx00000x

www.rsc.org/

Jickson Joseph,[a] Anjali Paravannoor,[a] Shantikumar V.Nair,[a] Zhao Jun Han,[b] Kostya (Ken)Ostrikov[b,c*] and Avinash Balakrishnan[a]*

Supercapacitor electrodes assembled from meso/macroporous camphor-derived carbon sponges show highly-promising performance in ac line-filtering. The coin-type supercapacitor exhibits ultrafast frequency response with a phase angle of -78^0 and a RC time constant of 319 µs at 120 Hz and may be a viable alternative to the presently dominant aluminium electrolytic capacitors.

The domestic ac electricity is generated at a frequency of either 50 or 60 Hz. However, when nonlinear loads are connected in the circuitry, higher-order harmonics (typically >120 Hz) can be induced, which are detrimental to the electronic devices in use.[1] This problem is rectified by using aluminium electrolyte capacitors (AECs) in the ac line-filtering, which provide buffers to filter out higher-order harmonics and protect against electrical power surges and spikes in automobile, portable electronic, and medical devices.[2-4] However, because of their low specific capacitance, AECs often occupy the largest space and volume in the electronic circuits.

Supercapacitor is an emerging type of capacitive device with very high specific capacitance (usually 2–5 orders of magnitude higher as compared to that of AECs). It shows great promise to replace AECs inac line filter by significantly reducing the size and volume of capacitive components.[5-8] However, in most cases, supercapacitor behaves like a resistor at 120 Hz when introduced into the transmission lines.[4] This poor frequency response is mainly due to the high RC time constant (>0.1 s) associated with the high electrochemical series resistance and the microporous structure of supercapacitor electrodes.[5-8] It is thus necessary to improve the frequency response of supercapacitor before it can be implemented in ac line filter.

A range of materials including onion-like carbon, carbide derived carbon, polymers, and metal oxides have been explored to fabricate the electrodes for supercapacitors with improved frequency response.[9-12] In particular, graphene and carbon nanotubes (CNTs) have shown promising performance for high-rate supercapacitors.[4,13-19] Nevertheless, the fabrication methods associated with graphene and CNTs suffer from high cost and complicated processes. Moreover, graphene sheets and carbon nanotubes often aggregate when immersed in the electrolyte due to the strong van der Waals' interactions, resulting in excessive inaccessible pores and impaired ion transport.[15,16,20–24]

The frequency response of supercapacitor can be generally tackled by fabricating high surface area electrodes with meso/macroporous structure and controlled pore size distribution.[25,26] In this work, we report for the first time a highly conductive carbon sponge exhibiting meso/macroporous structure. The material is obtained *via* the pyrolysis of camphor, a low cost source of carbon, followed by a facile freeze-drying approach to control the porosity through varying surfactant concentration. The carbon sponges show a typical 3-D hierarchical structure with tuneable distribution of meso- and macro-pores, facilitating good ion mobility and fast ion transport for supercapacitor applications.

All the chemicals used in the present study were of reagent grade obtained from Nice Chemicals, India. Carbon nanobeads, obtained by pyrolyzing camphor in air, were used as the starting material for synthesizing carbon sponges.[27] The morphology, size distribution, XRD and Raman spectra, and the formation mechanism of camphoric carbon nanobeads are given in the ESI Figures S1 and S2. Then, 100 mg carbon nanobeads were blended in waterwith 1 wt% PVA binder and

sodium dodecyl sulphate (SDS) as thesurfactant. Depending on the concentration of surfactant, three samples S-1, S-2, and S-3 were prepared. These dispersed solutions were then lyophilized at -20 ºC for 24 h and the corresponding carbon sponges were obtained.

Morphological and structural characterizations were performed using scanning electron microscopy (SEM; JEOL, JSM-6390LV), high-resolution transmission electron microscopy (HR-TEM; JEOL, JEM-2100F), Fourier transform infrared spectroscopy (FT-IR; Thermo Nicolet, Avatar 370) and X-ray diffraction analyses (XRD; X'Pert PRO Analytical). Surface area measurements were carried out using a BET surface area analyzer (Quantachrome Nova). For the electrochemical characterizations, two-electrode coin-type cells (CR2032) were assembled by cutting the sponge samples into pieces of 16 mm in diameter. The mass loading of each single electrode was ~1.5 mg cm^{-2}. The electrodes were soaked in 1M KOH electrolyte. A polypropylene (PP; BATSOL) film was used as the separator. Activated carbon-based supercapacitors was also assembled in a conventional way as the control sample, where a slurry of activated carbon with PVDF as the binding polymer were used to fabricate the electrodes. Aluminium electrolyte capacitors (AECs) were purchased from Keltron, India. Cyclic voltammetry (CV), electrochemical impedance spectroscopy (EIS), and galvanostatic charge-discharge were performed to evaluate the performance of supercapacitor using an electrochemical workstation (Metrohm; Autolab PGSTAT302N).

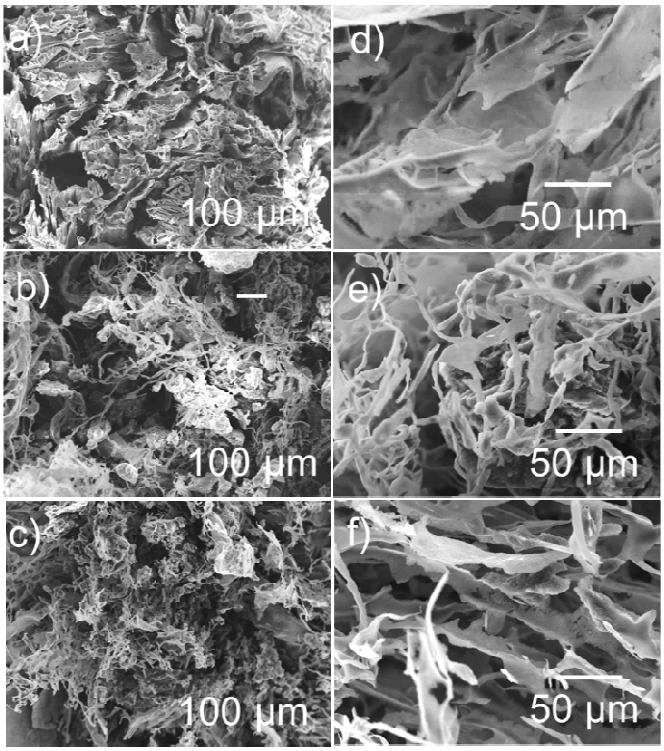

Figure 1. Carbon sponges prepared with SDS surfactant concentrations at (a,d) 0.5, (b,e) 0.75, and (c,f) 1 wt%.

Figure 1a-c shows the SEM images of carbon sponges of S-1, S-2 and S-3 lyophilized with different SDS surfactant concentrations at 0.5, 0.75 and 1 wt%, respectively. The density of samples was determined to be ~5–8 mg/cm^3. Figure 1d-f shows the magnified images of S-1, S-2, and S-3, respectively. It is observed that, as the surfactant concentration increased from 0.5 to 1 wt %, carbon sponge exhibited larger pores and a higher degree of meso/macroporosity. Raman spectra of the sponges showed similar D and G peaks as that of carbon nanobeads, indicating that no significant phase change occurred during the lyophilization process (ESI Figure S3). In addition, four-point probe measurements showed a high electrical conductivity of ~10 S cm^{-1} for these carbon sponge-based electrodes derived from camphor.

BET surface area analyses were also performed to investigate the porosity of the carbon sponges. Figure 2a shows the N_2 adsorption–desorption isotherms of carbon sponges S-1, S-2, and S-3. The isotherms displayed type IV isotherm with type H2 hysteresis, indicating a complex hierarchical porous network with anisotropic shapes. The surface area obtained for the samples S-1, S-2 and S-3 are 186, 213 and 248 m^2g^{-1}, respectively. As the concentration of SDS surfactant increased from 0.5 to 1 wt%, the hysteresis shifted to higher values of P/P_0, suggesting an increase of the maximum pore size. The associated increase in meso/macroporous volumes is considered beneficial for ionic conductivity.

Figure 2b shows the pore size distributions of carbon sponges S-1, S-2 and S-3. A broader size distribution with the peak shifting into the macroporous regime (>50 nm) was observed when the surfactant concentration was increased from 0.5 to 1 wt%. In particular, S-3showed a bimodal size distribution of pores in the mesoporous (2–50 nm) and macroporous (>50 nm) regimes. Clearly, surfactants played an important role to tailor the texture of porous carbon sponges. It is known that when the concentration of SDS is above the critical micellar concentration (CMC), a substantial aggregation of micelles could be induced.[28] These micelles are likely to be in spherical shapes and form cylindrical structures at a higher concentration, thereby shifting the pore size distribution of carbon sponges towards the macroporous regime after lyophilization.[29]

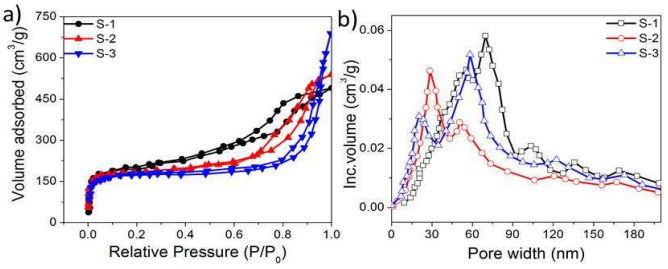

Figure 2. (a) Adsorption isotherms and (b) pore size distribution of all samples S-1, S-2, and S-3.

Symmetric coin-type cells in a two-electrode configuration were constructed using these sponges and the EIS spectra were

obtained at the frequency range of 0.1 Hz to 100 KHz.[30,31] Figure 3a shows the Bode plot of all carbon sponges. In general, the phase angle Φ at 120 Hz can be used as a "figure-of-merit" to evaluate the ac line-filtering performance.[4] One can see that when the SDS concentration was increased from 0.5 wt% of S-1 to 1 wt% of S-3, the phase angle Φ increased from -65° to -78° at 120 Hz, respectively. This indicated that the device behaved more like a capacitor rather than a resistor (Φ=-90^0 for ideal capacitor and Φ=0^0 for ideal resistor). Figure 3b compares the frequency response of S-3 with that of AEC and activated carbon-based supercapacitor.[32] The Φ of S-3 carbon sponge (-78°) was much larger that of activated carbon-based capacitor (~0°) and was comparable to that of AEC (85.5^0).[16] In addition, the resistance and reactance of the capacitor reach an equal value at the phase angle of -45^0. It is thus also important to compare the frequency of different electrodes at this phase angle. Notably, the impedance phase angle of S-3 reached -45^0 at 4.2 KHz, which was much higher than those of supercapacitors based on activated carbon (0.05 Hz)[29] or CNTs (636 Hz).[15]

Figure 3c-d shows the Nyquist plot of S-3, where a nearly vertical line was observed in the whole frequency region. The plot intersected with the real axis at an angle much larger than 45^0, suggesting the absence of microporous electrode behavior.[4] Moreover, a semicircle that is associated with charge transfer at the interface of electrode and electrolyte was not observed, indicating fast ion diffusion in the present case.

Because of the capacitive behavior at low frequencies, a series RC circuit model can be used to simulate the resistive and capacitive components of the electrode. In this model, capacitance can be calculated by *C=-1/(2πfZ")*, where *f* is the frequency in Hz and *Z"* is the imaginary part of the impedance spectrum.[6] As shown in Figure 3e, the capacitance increased from 5 to 269 μF cm^{-2} when the frequency was decreased from 10^5 to 10 Hz. The RC time constant was calculated to be 319 μs at 120 Hz, with the capacitance of 172 μFcm^{-2}and the resistance of 1.86 Ω as obtained from the Figure 3c. Such a small RC time constant of the sponge-based supercapacitor holds a great potential in ac line-filtering applications as the maximum time constant for filtering all the 5th and higher order harmonics (>120 Hz) is 8.3 ms.[33] Moreover, a specific capacitance (C_s) value of 172 μF cm^{-2} was obtained at 120 Hz, which is several times higher than that of the filters based on the bare nickel electrodes (25 μF cm^{-2})[2] or bare gold electrodes (11 μF cm^{-2}).[16] The ultrafast frequency response can be attributed to the larger pore size in the meso/macroporous carbon sponges induced at a higher surfactant concentration (see Figures 1 and 2). Moreover, the high C_s can be attributed to good ion adsorption with improved ion accessibility into the 3D interpenetrating macroporous structures.[4,16,34,35]

The minimal time required to fully discharge a supercapacitor with >50% of its peak value is the relaxation time constant τ_0 (note that this is different from the above RC time constant), which is obtained from the frequency at a maximum *C"*, the imaginary capacitance as depicted in Figure 3f.[31] τ_0 as low as 371 μs (*i.e.,* 2.7 kHz) was found for S-3 sample, confirming the fast ion diffusion of the system. This value is smaller than most of the previously reported high-rate supercapacitors based on various nanomaterials, such as onion-like carbon (26 ms),[9] multi-layered graphene film (13.3 ms),[14]and CNTs (1.5 ms).[18]

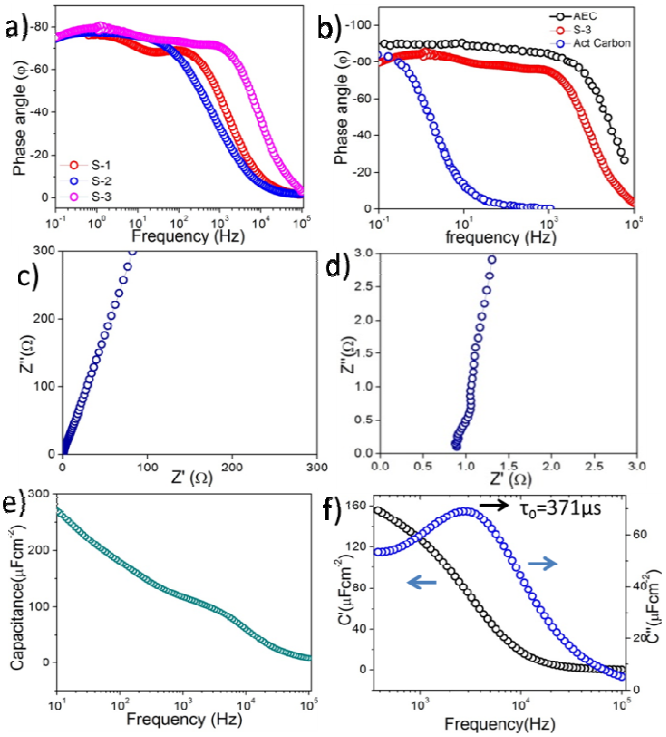

Figure 3.(a) Bode plots of the impedance phase angles for S-1, S-2, and S-3. (b) Comparison of the frequency response of S-3 with AEC and activated carbon-based supercapacitor. (c,d) Nyquist plot of S-3. (e) Specific capacitance and (f) real and imaginary parts of the capacitance of S-3 as a function of frequency.

Electrochemical characteristics of all the samples have also been analysed using CV tests at a scan rate of 20 mVs^{-1} in the 1M KOH electrolyte (ESI; Figure S4). All sponges showed symmetric curves resulting from the fast and reversible ion adsorption and desorption. As compared to the CV curves of commercial AECs (ESI; Figure S7), these curves showed reversible redox peaks with a shape that was deviated from the typical rectangular CV shape. This is due to the surface functional groups presented during the preparation of carbon sponges. To confirm this, FTIR spectrum of S-3 is shown in Figure S5 (ESI). The spectrum showed O-H stretching (3200-3400 cm^{-1}), C=O and C-O stretching (1629 cm^{-1}) and aromatic C=C stretching (1400-1600 cm^{-1}). The bands corresponding to anti-symmetric and symmetric stretching vibrations of =CH_2 were also seen at 2925 and 2853 cm^{-1}, respectively.[23] These vibrational bands indicated the presence of graphitic carbon as well as the residual oxygen functional groups, possibly resulted from the strongly oxidative atmosphere during the camphor pyrolysis. The presence of functional groups can not only improve the electrode wettability in aqueous electrolytes,

resulting in higher ion mobility and faster ion transport, but also contribute to the pseudocapacitance arising from the rapid Faradaic redox reactions.[36-38]

The areal specific capacitance was calculated from the CV curves using the following equation,

$$C = \frac{1}{A\Delta Vs}\int IdV \qquad (1)$$

Where C is the areal specific capacitance (F cm^{-2}), A is the area of the active electrode, ΔV is the voltage window, s is the scan rate and I is the current.[39,40] The areal capacitance was calculated to be 412, 471 and 487 μF cm^{-2} for samples S-1, S-2 and S-3, respectively. The charge/discharge curves of S-3 at different current densities are also shown in Figure S6 (ESI). Remarkable cycling stability with no significant degradation in capacitance was observed after 5,000 cycles of charging/discharging (ESI; Figure S6b). Furthermore, Table S1 compares the performance metrics of camphor-derived carbon sponge in the present study with other electrode materials reported in the recent literature (ESI). Our results are favourably comparable or better than many electrodes that are potential for replacing AECs in ultrafast frequency response devices.

In conclusion, we have developed a simple approach to synthesize porous carbon sponges wherein carbon was derived from the cheap source camphor. The pore size distribution of carbon sponges can be readily controlled by adding surfactant in the freeze-drying process. Supercapacitor using the carbon sponge as electrodes exhibited a phase angle of -78º and a RC time constant of 319 μs at 120 Hz, making it highly promising to replace AECs in ac line-filtering. Further improvement on capacitance can be made by optimizing the electrode fabrication as well as electrolyte.

Financial support from Department of Atomic Energy, Board of Research in Nuclear Sciences (BRNS), BARC, Grant No: 2013/37P/62/BRNS and Indian Space Research Organization (ISRO, Grant No: ISRO/RES/3/660/2014-15) are gratefully acknowledged. This work was partially supported by the Australian Research Council (DE130101264 and FT100100303) and CSIRO Science Leader Program.

Notes and references

[a]Nanosolar Division, Amrita Centre for Nanosciences, AIMS, Ponekkara, Kochi 682041, India

E-mail: avinash.balakrishnan@gmail.com

[b]CSIRO Manufacturing Flagship, P.O. Box 218, Bradfield Road, Lindfield, NSW 2070, Australia

E-mail: kostya.ostrikov@csiro.au

[c]School of Chemistry, Physics and Mechanical Engineering, Queensland University of Technology, Brisbane QLD 4000, Australia

†Electronic Supplementary Information (ESI) available. See DOI: 10.1039/c000000x/

1 A. Dale, C. Brownson, C. E. Banks, *Chemcomm.* 2012, **48,** 1425.
2 L. Zhang, X. Zhao, *Chem. Soc. Rev.,* 2009 **38,** 2520.
3 A. G. Pandolfo, A. F.Hollenkamp, *J. Power Sources,* 2006, **157,** 11.
4 J. R. Miller, R. A. Outlaw, B. C. Holloway, *Science,* 2010, **329,** 1637.
5 C. M. Niu, E. K. Sichel, R. Hoch, D. Moy, H. Tennent, *Appl. Phys. Lett.*, 1997**, 70,** 1480.
6 Y. Honda, T. Haramoto, M. Takeshige, H. Shiozaki, T. Kitamura, M. Ishikawa, *ElectrochemSolid-State Lett.,* 2007, **10,** A106-A110.
7 J. W. Long, B. Dunn, D. R. Rolison, H. S. White, *Chem. Rev.,* 2004, **104,** 4463.
8 D. R. Rolison, J. W. Long, J. C. Lytle, A. E. Fischer, C. P. Rhodes, T. M. McEvoy, A. M. Lubers, *Chem. Soc. Rev.,* 2009, **38,** 226.
9 D. Pech, M. Brunet, H. Durou, P. Huang, V. Mochalin, Y. Gogotsi, P. Simon, *Nature Nanotech.,* 2010, **5,** 651.
10 Y. Korenblit, M. Rose, E. Kockrick, L. Borchardt, A. Kvit, S. Kaskel, G. Yushin, *ACS Nano*, 2010, **4,** 1337.
11 Y. Hou, Y. Cheng, T. Hobson, J. Liu, *Nano Lett.,* 2010, **10,** 2727.
12 X. Lang, A. Hirata, T. Fujita, M. Chen, *Nature Nanotech.,* 2011, **6,** 232.
13 Y. Zhu, S. Murali, M. D. Stoller, K. J. Ganesh, W. Cai, P. J. Ferreira, R. S. Ruoff, *Science,* 2011, **332,** 1537.
14 X. Yang, J. Zhu, L. Qiu, D. Li, *Adv. Mater.,* 2011, **23,** 2833.
15 C. Liu, Z. Yu, D. Neff, A. Zhamu, B. Z. Jang, *Nano Lett.,* 2010, **10,** 4863.
16 K. Sheng, Y. Sun, C. Li, W. Yuan, G. Shi, *Sci. Rep.,* 2012, **2,** 247.
17 D. N. Futaba, K. Hata, T. Yamada, T. Hiraoka, Y. Hayamizu, Y. Kakudate, S. Iijima, *Nature Mater.,* 2006, **5,** 987.
18 C. Du, N. Pan, *J. Power Sources,* 2006, **160,** 1487.
19 Z Bo, W Zhu, W Ma, Z Wen, X Shuai, J Chen, J Yan, Z Wang, K Cen, X Feng, *Adv. Mater.*, 2013, **25**, 5799.
20 J. J. Yoo, K. Balakrishnan, J. Huang, V. Meunier, B. G. Sumpter, A. Srivastava, P. M. Ajayan, *Nano Lett.,* 2011, **11,** 1423.
21 R. Ranjusha, S Ramakrishna, A.S. Nair, P. Anjali, S. Vineeth, T. S. Sonia, N. Sivakumar, K. R. V. Subramanian, S V. Nair and A. Balakrishnan. *RSC Adv.,* 2013, **3,** 17492.
22 D. Zhang, X. Wen, L. Shi, T. Yan and J. Zhang, *Nanoscale,*2012, **4,** 5440.
23 R. Ranjusha, A. Sreekumaran Nair, S. Ramakrishna, P. Anjali, K. Sujith, K. R. V. Subramanian, N. Sivakumar, T. N. Kim, S. V. Nair and A. Balakrishnan, *J. Mater. Chem.,* 2012, **22,** 20465.
24 A. C. Ferrari and J. Robertson, *Phys. Rev. B,* 2001, **64,** 075414.
25 X. Wang, Y. Zhang, C. Zhi, X. Wang, D. Tang, Y. Xu, Q. Weng, X. Jiang, M. Mitome, D. Golberg, Y. Bando, *Nat. Comm.,* 2013, 4, 2905.
26 J. H. Lee, N. Park, B. G. Kim, D. S. Jung, K. Im, J. Hur, J. W. Choi, *ACS Nano,* 2013, 7, 9366.
27 A. Paravannoor, A. S. Nair, R. Ranjusha, Pattathil Praveen, K. R. V. Subramanian, N. Sivakumar, S. V. Nair, A. Balakrishnan, *ChemPlusChem,* 2013, **78,** 1258.
28 I. Matos, S. Fernandes, L. Guerreiro, S. Barata, A. M. Ramos, J. Vital, I. M. Fonseca, *Micropor. Mesopor. Mater.,* 2006, **92,** 38.
29 M. Bourrel, R. Scheter, Microemulsions and Related Systems, *Formulation, Solvency and Physical Properties*, Marcel Dekker, New York and Basel, 1998, 31.
30 M. D. Stoller, R. S. Ruoff, *Energy Environ. Sci.,* 2010, 3, 1294.
31 J. Feng, X. Sun, C. Wu, L. Peng, C. Lin, S. Hu, J. Yang, Y. Xie, *J. Am. Chem. Soc.,* 2011, **133,** 17832.
32 D. Qu, H. Shi, *J. Power Sources,* 1998, **74,** 99
33 P. L. Taberna, P. Simon, J. F. Fauvarque, *J. Electrochem. Soc.,* 2003, **150,** A292.
34 L. Zhang, F. Zhang, X. Yang, G. Long, Y. Wu, T. Zhang, K. Leng, Y. Huang, Y. Ma, A. Yu, Y. Chen, *Sci. Rep.,* 2013, 3, 1408.
35 P. Si, S. Ding, X. W. Lou D. H. Kim, *RSC Adv.,* 2011, 1, 1271.

36 M. D. Stoller, S. Park, Y. Zhu, J. An, R. S. Ruoff, *Nano Lett.,* 2008, **8,** 3498.
37 T. Brousse, M. Toupin, D. Bélanger, *J. Electrochem. Soc*., 2004, **151**, A614.
38 V. Khomenko, E. Raymundo-Piñero, F. Béguin, *J. Power Sources,* 2006, **153**, 183.
39 J. Lin, C. Zhang, Z. Yan, Y. Zhu, Z. Peng,R. H. Hauge,D.Natelson, J. M. Tour, *Nano Lett.*, 2013, **13,** 72.
40 M. F. El-Kady, V. Strong, S. Dubin, R. B. Kaner, *Science*, 2012, **335**, 1326.